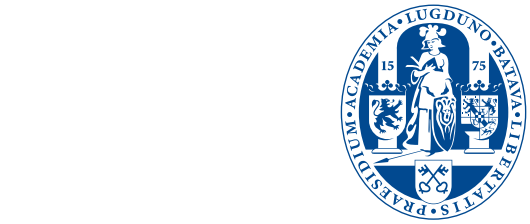

Implementing NanoSQUIDs for Detection of Quantum Phase Fluctuations

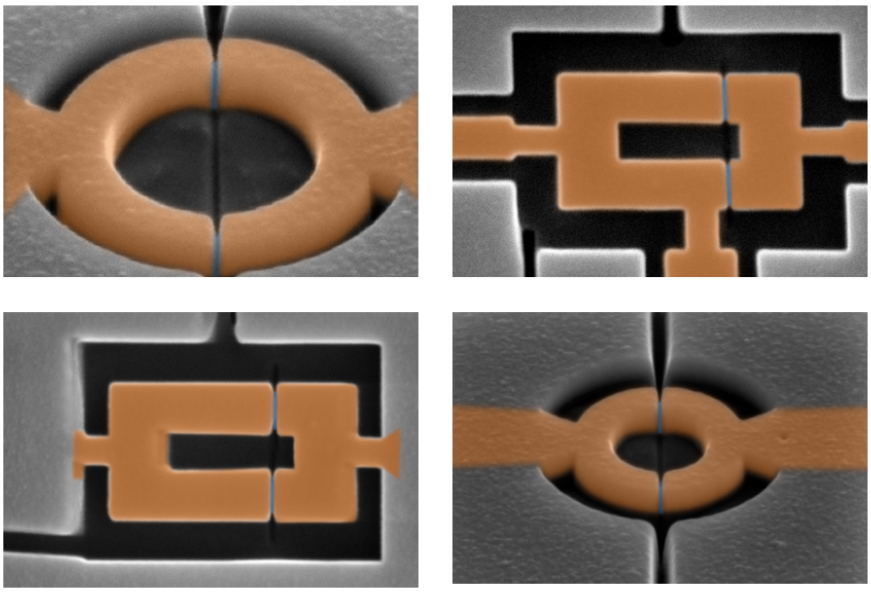

Thesis

submitted in partial fulfillment of the
requirements for the degree of

Master of Science
in
Physics

Author :	Yasmin Charlotte Doedes
Student ID :	s2028638
Supervisor :	Matthijs Rog, MSc
	Dr. Kaveh Lahabi
Second corrector :	Dr. Ir. Bas J. Hensen

Leiden, The Netherlands, February 23, 2024

Implementing NanoSQUIDs for Detection of Quantum Phase Fluctuations

Yasmin Charlotte Doedes

Leiden Institute of Physics, Leiden University
P.O. Box 9500, 2300 RA Leiden, The Netherlands

February 23, 2024

Abstract

Quantum phase transitions (QPTs) occur in a large variety of systems, including disordered superconductors and quantum magnets. Because of accelerated developments in quantum technology, understanding these materials is becoming increasingly important. Studying the quantum phase fluctuations (QPFs) that occur close to QPTs in these materials is especially important for understanding quantum critical behavior. In order to locally probe QPFs in disordered superconductors, we develop an AC magnetic susceptibility measurement scheme based on nanoSQUIDs (Superconducting Quantum Interference Devices). Using this measurement scheme with a single SQUID, we confirm that we have sufficiently high sensitivity to measure QPFs. To answer open questions about the spatial and temporal nature of QPFs around a QPT, we propose a multi-SQUID setup that can measure correlations in susceptibility across different length- and time scales. The first step towards the multi-SQUID setup has been made by the fabrication of a two-SQUID device and the outline of an accompanying measurement protocol.

Contents

Chapter 1

Introduction

1.1 Quantum Phase Fluctuations

Quantum phase fluctuations (QPFs) are a purely quantum mechanical phenomenon and a direct result of Heisenberg's uncertainty principle. QPFs can be found around quantum phase transitions (QPTs), which occur in a large variety of systems. Examples of QPTs are metal-insulator transitions found in disordered alloys [1], Quantum-Hall transitions [2], magnetic transitions in quantum magnets [3, 4] and superconductor-insulator transitions in disordered superconductors [5–7], see Fig. 1.1.

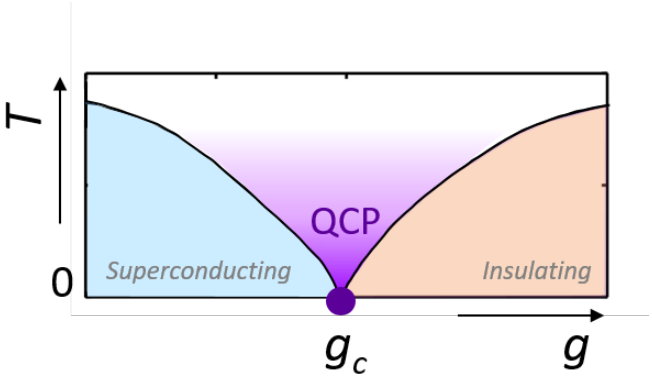

Figure 1.1: The phase diagram of the SIT, a type of QPT, found in disordered superconductors. At $T = 0$ K, the system can be tuned from superconducting to insulating as a function of the non-thermal tuning parameter g. In the case of a SIT, g can be the degree of disorder or external magnetic field strength. Although the transition occurs strictly at the quantum critical point (QCP, $g = g_c$), the QPFs that drive the transition are present in a region of non-zero temperature around the QCP (purple), called the quantum critical region.

Quantum materials, which are materials that cannot be described by a single-particle picture, have been found to exhibit signs of QPFs over macroscopic length scales. These materials have gained increased attention because of their promising applications in quantum technologies and because of advancements in fabrication techniques and metrology. To optimally exploit this class of materials, it is beneficial to form a better understanding of them, especially regarding the QPTs that they exhibit.

Despite theoretical efforts, QPTs are far from being fully understood. Not only are

there questions concerning the exact mechanism behind specific QPTs, but also more fundamental questions applying to all QPTs are unanswered. For example, what are the length and time scales associated with QPFs around a quantum critical point (QCP)? It is well-known that the size of QPFs diverges towards the QCP, but there is no complete and universal scaling theory. Since all QPTs are described by the same physics, answering such questions for one specific system will provide insights for all systems with a QPT. Experimental observation of QPFs near a QCP could therefore be of great value.

In this thesis, we design and test an experimental setup that will be used to gain insight into the spatial and temporal nature of QPFs near a QCP. We propose a multi-nanoSQUID (Superconducting Quantum Interference Device) setup that can simultaneously measure magnetic susceptibility as a function of time at different locations on a thin-film disordered superconductor. When these SQUIDs are separated by a variety of distances, the correlations among the susceptibility measured by the individual SQUIDs, will reveal information about the length and time scales of the QPFs.

1.2 The Superconductor-Insulator Transition

QPTs occur in materials that have competing ground states at zero temperature. These ground states are called quantum phases. Such systems can be tuned from one quantum phase to another by changing a certain physical parameter, g, that is not the temperature. This transition is driven by QPFs, as opposed to thermal fluctuations. Although a direct QPT only occurs at zero temperature, the phase transition influences the phase diagram over a wide range of temperatures in what is called the quantum critical region, or region of criticality. Throughout this region, QPFs are present. However, with rise in temperature, the QPFs become increasingly hard to detect as they will be buried in thermal fluctuations.

Disordered superconductors are a class of materials that exhibit an electronic QPT that has been studied for several decades. In 1990, Fisher predicted that disordered 2D superconductors have a zero-temperature SIT [8]. He described this with a scaling theory. Shortly after, the transition was observed in low-temperature transport measurements in 2D thin films of MoGe, a disordered superconductor [9]. The data showed a transition in the zero bias resistance as a function of external field strength, largely (but not fully) consistent with the scaling theory proposed by Fisher.

Phase transitions can be either first-order or second-order. In the former, the change from one phase to the other is very sudden, whereas for a second-order transition, this change is continuous. SITs are second-order phase transitions. A defining characteristic of such phase transitions is the divergence of the characteristic length scale of the QPFs at the QCP, $g = g_c$. This can be explained as follows [10]: the wavefunction at both sides far away from the QCP is described by a product state of simple states. As the QCP is approached, the state becomes more complicated as more and more QPFs appear. Right at the transition, $g = g_c$, the state is described by an involved quantum superposition containing an exponentially large set of configurations that fluctuate at all length scales.

On one end of a SIT lies a superconductor. Superconductivity is described by a complex order parameter, $\Psi = |\Psi|e^{i\phi}$, consisting of an amplitude, $|\Psi|$, indicating the Cooper pair density and phase, ϕ, indicating the coherence and thus superfluid density. In dis-

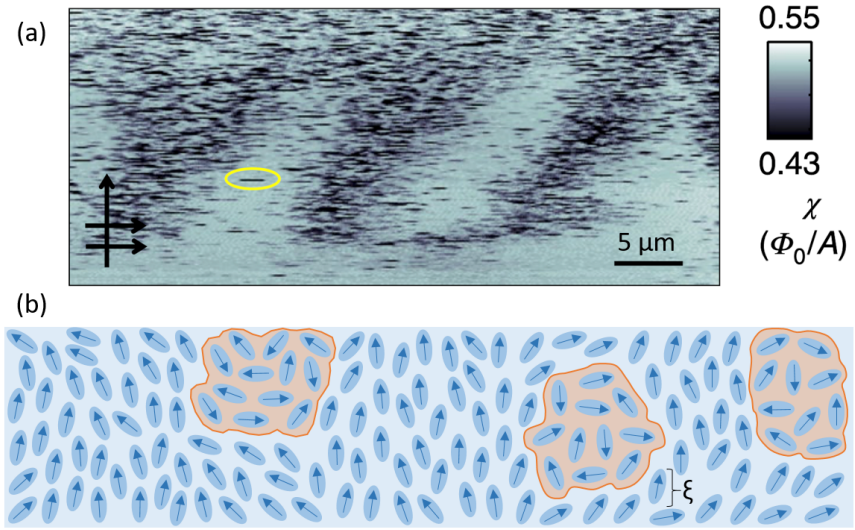

Figure 1.2: **(a)** Spatial map of the QPFs on the superconducting side of the SIT in NbTiN, imaged with scanning SQUID susceptometry [7]. The darker regions correspond to regions of suppressed superconductivity and thus the QPFs. The streaks (encircled in yellow) are artifacts of scanning. **(b)** Cooper pairs (indicated by blue ovals, with a characteristic size equal to the coherence length, ξ) exist in both the superconducting and insulating state around a SIT. However, only in the superconducting state are these Cooper pairs phase coherent (arrows pointing in roughly the same direction). In the insulating state, the Cooper pairs are phase incoherent (arrows pointing in random directions). The orange patches indicate QPFs on the superconducting side of a SIT.

ordered superconductors, the order parameter shows spatial fluctuations, leading to the creation of superconducting islands [11, 12]. In conventional superconductors, this is not the case. The uniformity of the order parameter in space gives rise to superconducting behavior in conventional superconductors. Yet, disordered superconductors also exhibit zero resistance as long as the amplitude is non-zero everywhere and the phase across the sample is correlated. These conditions ensure that Cooper pairs can tunnel from one superconducting island to another, thereby establishing superconducting behavior.

The exact nature of the SIT in disordered superconductors has been debated. It has been shown that the mechanism of transition differs between moderately and strongly disordered superconductors [12]. When driving a moderately disordered superconductor through its QCP by increasing the external magnetic field strength, insulating behavior sets in because of suppression of the order parameter's amplitude, while phase correlations outlast nonzero amplitude. In highly disordered superconductors, on the other hand, phase coherence breaks while the amplitude remains nonzero. This would imply that there are still Cooper pairs present in the insulating state. More recent low-temperature scanning tunneling spectroscopy and magnetotransport measurements on MoGe films have shown to be consistent with phase incoherent Cooper pairs once the film is on the insulating side of the SIT transition [13–15].

A local visualization of the QPFs in space and time could help to create a better understanding of the SIT. The first (and the time of writing, the only) results of such measurements have been published for the disordered superconductor NbTiN [7], see Fig.

1.2. In this research, scanning SQUID susceptometry is used to locally probe the superfluid density of three samples of NbTiN on the superconductor side of the SIT. Scanning SQUID susceptometry combines the high magnetic field sensitivity of a scanning SQUID with a locally applied AC magnetic field. When the probe is above a superconducting region, the externally applied field will be suppressed. In this case, the SQUID measures a smaller magnetic field compared to when it is above an insulating region, where the field is not suppressed.

For NbTiN, the SIT is tuned by changing the degree of disorder, or film thickness. The transition was tuned from superconducting to insulating. As the QCP was approached, regions of suppressed superconductivity grew in size. The fluctuations exist well below the SC transition, persisting in a regime in which thermal fluctuations were expected to be sufficiently suppressed. Moreover, fixed-position time traces were recorded, which remarkably showed real-time quantum phase fluctuations over a wide range of characteristic times, from milliseconds to minutes. Of course, this surprising finding raises even more questions about the temporal nature of QPFs.

1.3 Outline

The first visualization of QPFs in the disordered superconductor NbTiN, as mentioned in the previous section, has surely been a remarkable step towards a better understanding of QPTs. However, to learn more about the spatial and temporal nature of QPFs around QPTs, it is essential to measure correlations. This requires simultaneously measuring with several probes. This thesis will discuss steps towards the design and testing of such a measurement scheme.

In chapter 2, AC magnetic susceptibility is introduced as a suitable measure for the phase coherence of Cooper pairs. The use of nanoSQUIDs to measure AC susceptibility is discussed as well. In the next chapter, 3 the fabrication process of our nanoSQUID susceptometers is outlined. This chapter also briefly mentions how SQUIDs should be operated and on what parameters the field sensitivity of the SQUID depends. In section 3.3, the use of kinetic inductance as opposed to geometric inductance to bias a SQUID is elaborated on, as this technique is useful for the operation of multi-SQUID devices.

The first measurement results are discussed in chapter 4. The indirect detection of a change in magnetic response of a thin Nb film going through a broad superconducting transition will be presented. Since the change in magnetic response is expected to be very small for this particular Nb film, these results confirm that we can measure very small susceptibility signals, including QPFs.

In the next chapter, 5, the development of an AC susceptibility measurement scheme is detailed. First, a protocol to measure with a single SQUID is developed and tested. Test measurements are performed on two Nb films that go through a superconducting transition. The measurement results are unexpected and provide new insights into SQUID-biasing and -stability. This chapter ends by presenting a two-SQUID device and measurement scheme to simultaneously measure AC susceptibility at two separate locations on a film. No measurements are performed with this device. An overview of all findings and conclusions, and an outlook will be given in the final chapter, 6.

Chapter 2

Magnetic Susceptibility Measurements

In the previous chapter, QPFs and SITs in disordered superconductors were introduced. Both the superconducting and insulating state around the SIT host Cooper pairs. But only in the superconducting state are these Cooper pairs phase coherent and have the ability to repel an external magnetic field. Therefore, the visualization of QPFs around a SIT relies on locally probing the magnetic response. This chapter will introduce the AC magnetic susceptibility, χ, as a suitable measure. Also, the use of nanoSQUIDs to perform these measurements will be elaborated on.

2.1 Magnetic Susceptibility

When a magnetic field, H, is applied to a material, it might respond by changing its magnetization, M. Not all materials have a magnetic response. The magnetic susceptibility, χ, is a measure of a material's magnetic response as a function of the applied magnetic field. Generally, for small fields, the response is linear, which leads to the following expression for the susceptibility:

$$\chi = M/H \tag{2.1}$$

Materials that align their magnetization with the external field, $\chi > 0$, are called paramagnets. An opposite response, $\chi < 0$, is called diamagnetism. Superconductors shield all external field (up to a critical field strength) and are therefore referred to as perfect diamagnets, $\chi = -1$. However, in thin film superconductors, there might not always be enough space for the phase of the order parameter to bend and create sufficient screening currents. Lastly, insulators are a type of material that does not have a magnetic response, $\chi = 0$.

In many scenarios, the magnetic response of a material is not linear and the earlier expression for the susceptibility is no longer applicable. A more general measure of magnetic response is the differential susceptibility (also called AC susceptibility):

$$\chi = \mathrm{d}M/\mathrm{d}H \tag{2.2}$$

The differential susceptibility is measured in AC susceptibility experiments, where an oscillating magnetic field is applied to a sample. There are two main advantages of measuring the AC susceptibility instead of the linear susceptibility. First of all, in an AC measurement the slope instead of the absolute value of $M(H)$ is measured, which enhances the sensitivity. Secondly, sensitivity can be improved even more by using lock-in

techniques.

When applying a time-dependent field, a time-dependent magnetic moment is induced:

$$M(\mathrm{t}) = \chi H \sin(\omega \mathrm{t}) \tag{2.3}$$

In the equation above, H is the amplitude of the applied oscillating magnetic field and ω is the frequency of this oscillation. Especially at higher frequencies, dynamic effects in the sample might cause the magnetic response of the sample to be delayed with respect to the applied field. For this reason, an AC susceptibility measurement yields both an in-phase and out-of-phase component:

$$\chi = \chi' + i\chi'' \tag{2.4}$$

When measuring the AC susceptibility of superconducting films, both components have a distinct meaning [16]. χ' is a measure of the superfluid response. The superfluid response is in phase with the applied field since the response time of the Meissner currents is orders of magnitude smaller than one field oscillation (assuming kHz oscillations). More screening results in a larger absolute value of the magnetization and thus a larger absolute value of the susceptibility.

The out-of-phase component of the susceptibility quantifies energy dissipation. One of the mechanisms through which energy can be dissipated in superconducting films is the motion of vortices in response to screening currents. The movement of the vortices' normal cores dissipates energies. Close to the critical temperature, T_c, there are more vortices as the lower critical field goes to zero. Therefore, the out-of-phase component has a peak around T_c, with the peak being a measure of the sample's superconducting homogeneity.

2.2 NanoSQUIDs for Magnetic Susceptibility Measurements

One method of measuring (AC) susceptibility is the two-coil mutual inductance technique in which two coils are placed on opposite sides of a sample. One of these coils generates an (AC) magnetic field, which generates a current through the other. This current is a measure of the susceptibility of the film. A superconducting film placed in between the coils will (partially) screen the applied field and therefore reduce the current induced in the second coil. The two-coil mutual inductance technique has been applied in [17] to measure the magnetic penetration depth and phase stiffness superfluid response of overdoped copper oxides as a function of temperature and doping.

However, with this method the superfluid response is not measured locally, but for the entire film. To measure the QPFs around a SIT, we need a sensor that can locally measure magnetic response. Moreover, the sensitivity should be sufficient to measure small fluctuations. NanoSQUIDs are an appropriate sensor as they fulfill both requirements.

A SQUID is a ring of superconducting material interrupted by two Josephson junctions, see Fig. 2.1a. For nanoSQUIDs, this ring is smaller than a micron. The superconducting condensates on either side of a junction are described by their own complex order parameter, Ψ. The junctions are areas of suppressed superconductivity where the order parameters of both superconducting condensates overlap. Despite the suppressed

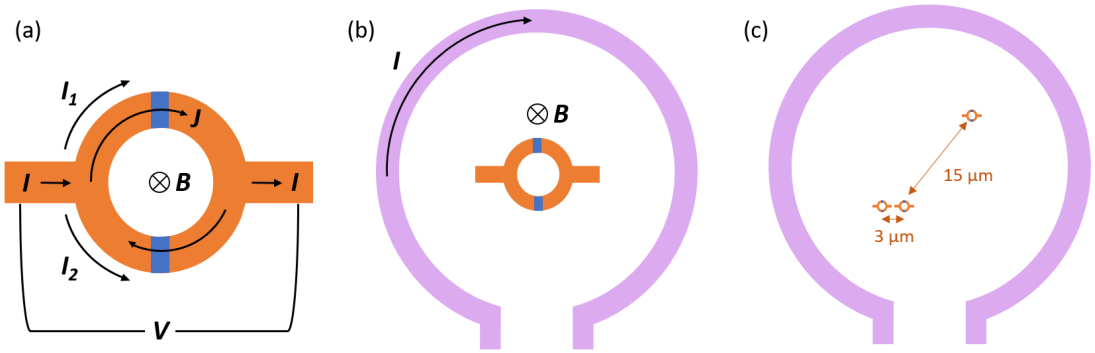

Figure 2.1: **(a)** A SQUID consists of a superconducting ring (orange) interrupted by two parallel Josephson junctions (blue). The SQUID is biased with a current, I, and given the right conditions, a voltage, V, can be measured across it. An extra circular supercurrent, J, can be induced by a magnetic field that is perpendicular to the SQUID. This circular current, and thus the voltage across the SQUID, are periodic in the external magnetic field. **(b)** Adding a FC concentric to the SQUID transforms the device into a susceptometer. By running a current, I, through the FC, a magnetic field is created. When this is an oscillating field, the differential susceptibility of a film that is deposited on top of the device (not shown) can be measured with the SQUID. **(c)** To investigate the temporal and spatial nature of QPFs in disordered superconductors, we want to measure correlations in susceptibility over different length- and time scales. Such a measurement can be performed with a setup as shown, that records time traces of magnetic response with at least three SQUIDs that are separated by different distances.

superconductivity, supercurrent can flow through the junctions, and therefore through the entire SQUID. To understand the SQUID's sensitivity to magnetic fields, two characteristics need to be pointed out.

First of all, the supercurrent that can flow through a junction is determined by the phase difference between the two superconducting condensates, this is described by the first Josephson relation. There is a maximum supercurrent, called the critical current, I_c, that can flow through a junction before a voltage starts to develop across it. This voltage is related to the time evolution of the phase difference. The second Josephson relation describes this.

Secondly, a superconducting ring, and therefore also a SQUID, requires fluxoid quantization. When the fluxoid state does not correspond to an integer multiple of 2π (or equivalently, an integer multiple of the magnetic flux quantum, $\Phi_0 \approx 2.07e^{-15}$ Wb), a compensating supercurrent, J, will be induced in the ring. This fluxoid quantization will be further elaborated on in section 3.3. The compensating supercurrent is periodic in the external magnetic flux. When there are two parallel junctions in the ring, a change in supercurrent leads to a change in phase difference (first Josephson relation) and therefore also a change in voltage (second Josephson relation). Consequently, the voltage across a SQUID is periodic in the magnetic flux. The magnetic flux, Φ, is related to the magnetic field, B, by the effective SQUID area, A_{eff}:

$$\Phi = BA_{\text{eff}} \tag{2.5}$$

To transform a SQUID from a magnetometer to a susceptometer, a field coil can be added concentric to the SQUID, see Fig. 2.1b. Such a field coil has a single winding and running a current, I, through it will create a perpendicular magnetic to and therefore a

flux through the SQUID. The SQUID measures the mutual inductance, M:

$$M = \Phi / I \tag{2.6}$$

By combining this expression for the mutual inductance with the definition of susceptibility and the equation for the magnetic field due to a circular current, we find that:

$$\chi = \frac{2RM}{\mu_0 A_{\text{eff}}} - 1 \tag{2.7}$$

In the equation above, R is the radius of the FC, M is the mutual inductance, and μ_0 is the vacuum permeability.

Two parameters determine a SQUID's performance: the spatial resolution and the magnetic field resolution [18]. The magnetic field resolution is limited by the magnetic field noise, S_B, which depends on the SQUID's effective area and the magnetic flux noise, S_Φ:

$$\sqrt{S_B} \approx \sqrt{S_\Phi} / A_{\text{eff}} \tag{2.8}$$

The magnetic flux noise is ultimately determined by the current noise in the junctions.

The spatial resolution depends on the effective SQUID area and separation from the sample. Of course, we need high spatial resolution to detect QPFs. A small effective area can for example be achieved by using a SQUID-on-tip approach. It is demonstrated that SQUIDs with a diameter just below 50 nm can be fabricated on pulled quartz tubes [19]. SQUID-on-tip can also achieve small sample-probe separation (up to 10 nm). However, this approach requires a scanning setup and is challenging to integrate with a field coil.

Another approach to ensure a small effective pick-up area is coupling a micron-sized SQUID to a sub-micron-sized pick-up loop. In such a configuration the field sensing area is fabricated some distance away from the junctions. This approach has been used in [7], where the earlier mentioned QPFs in NiTiN were imaged, and in [16], where a thin Nb film going through its superconducting transition was investigated. In both studies, the SQUID and pick-up loop were fabricated on a chip that was scanned over a sample.

Perhaps the simplest approach, regarding both producing and operation, is fabricating a nanoSQUID and depositing the film of interest on top. The sensor-sample separation in this case depends on the thickness of an intermediate insulating layer, which can be at least as thin as 50 nm.

For this research, this direct-deposition method will be used to investigate QPFs in disordered superconductors. Sputtered SiO_x is used as an insulating layer between the sensor and film of interest. When the film of interest is deposited on the nanoSQUID, the magnetic response can be measured very locally. By using a system consisting of at least three SQUIDs that are separated at different length scales, we can measure correlations as a function of time, see Fig. 2.1c. These correlations could reveal new insights into the characteristic length- and timescales of QPFs.

Chapter 3

SQUID Fabrication and Operation

The nanoSQUIDs that are used during this thesis are fabricated using electron-beam (e-beam) lithography and focused ion beam (FIB) milling. The latter technique allows for the creation of junctions as small as 15 nm. The entire fabrication process takes roughly three to four days.

Before the SQUIDs can be used in an experiment, they need to be characterized. It needs to be verified that the device shows critical current oscillations and has a sufficiently high transfer function. This chapter will cover how SQUIDs must be operated to characterize them and use them in experiments.

3.1 Design and Fabrication

To locally measure susceptibility, we have decided to use a sensor consisting of a nanoSQUID and FC concentric to it. Of course, this FC needs to generate sufficiently high fields at the SQUID area. In [7], where the QPFs accompanying the SIT of NiTiN were imaged with a similar probe, oscillating fields with an amplitude varying between 0.01 and 0.5 mT were applied. In our experiments, the sample-sensor separation is expected to be at least a factor 10 smaller, such that field strengths at the lower end of this range should be sufficient. When designing the FC, both field uniformity and the critical current of the structure should be taken into account.

All devices are produced on Si/SiO_x chips. In the first step of the fabrication process, e-beam lithography is used to create the pattern for the FC, the 'finger' in the center of the FC on which the nanoSQUID will be structured, and the contacts. The next step is thin film deposition with UHV magnetron sputtering. First, a layer of copper (Cu) ($\pm$ 20 nm) is deposited, followed by a layer of niobium (Nb) ($\pm$ 60 nm for SQUIDs B and C, $\pm$ 80 nm for the two-SQUID device). After the lift-off step, Ga^+ FIB milling is used to create the SQUID. A focused Ga-ion source very locally removes material, achieving feature sizes as small as 15 nm. To create the ring structure of the SQUID, sections of both Nb and Cu are milled. The junctions are created by only milling the Nb, such that superconductor-normal metal-superconductor (SNS) junctions are created.

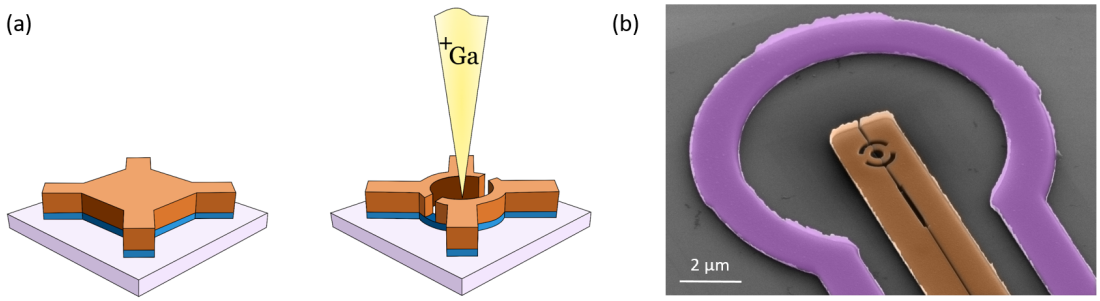

Figure 3.1: **(a)** Our devices consist of Cu (blue) and Nb (orange) on a Si/SiO_x chip. To create the SQUIDs, we use a Ga^+ FIB to mill material and create structures as small as 15 nm. The junctions are fabricated by only milling the Nb, thereby creating SNS junctions. Image from [20]. **(b)** False-colored SEM image of SQUID B (on the tip of the orange finger) surrounded by the FC (purple). The SQUID has a diameter of roughly 900 nm.

3.2 Operation

In section 2.2 it was stated that the voltage across a SQUID is periodic in the external magnetic field. Of course, the SQUID must be biased with a current such that the addition of an induced supercurrent, J, will exceed the critical current, and a voltage, also periodic in the external field, can be measured. The change in voltage as a function of the change in magnetic field is called the transfer function. The SQUIDs fabricated for this project have transfer functions as high as 24.9 mV/Φ_0, roughly 100 times higher than the transfer functions of conventionally used nanoSQUIDs [21].

Properly biasing a SQUID is essential in optimizing its sensing abilities. The transfer function of a SQUID depends on the temperature, fluxoid state (usually solely determined by the external magnetic field strength), and the bias current.

3.3 Modulation Lines for Field Biasing

As mentioned before, mesoscopic superconducting rings, and therefore also SQUIDs, require fluxoid quantization [22, Appendix 1]:

$$n\Phi_0 = \mu_0\lambda_L^2 \oint \vec{j}_s \mathrm{d}\vec{l} + \Phi_a \tag{3.1}$$

In the equation above, λ_L is the London penetration depth, j_s is the circular supercurrent density that is integrated along the ring, and Φ_a is applied flux. Generally, the supercurrent density is exponentially small. In that case, the fluxoid quantization requirement reduces to:

$$n\Phi_0 = \Phi_a \tag{3.2}$$

However, when the kinetic inductance of the SQUID is significant, the contribution of the circulating supercurrent to the fluxoid quantization cannot be neglected. The total flux through the SQUID is given by:

$$\Phi_{tot} = \Phi_a + LJ = BA_{\mathrm{eff}} + (L_{\mathrm{g}} + L_{\mathrm{kin}})J \tag{3.3}$$

In the equation above, L is the total inductance, L_{g} is the geometric inductance, and L_{kin} is the kinetic inductance. The total flux associated with a SQUID should equal an integer

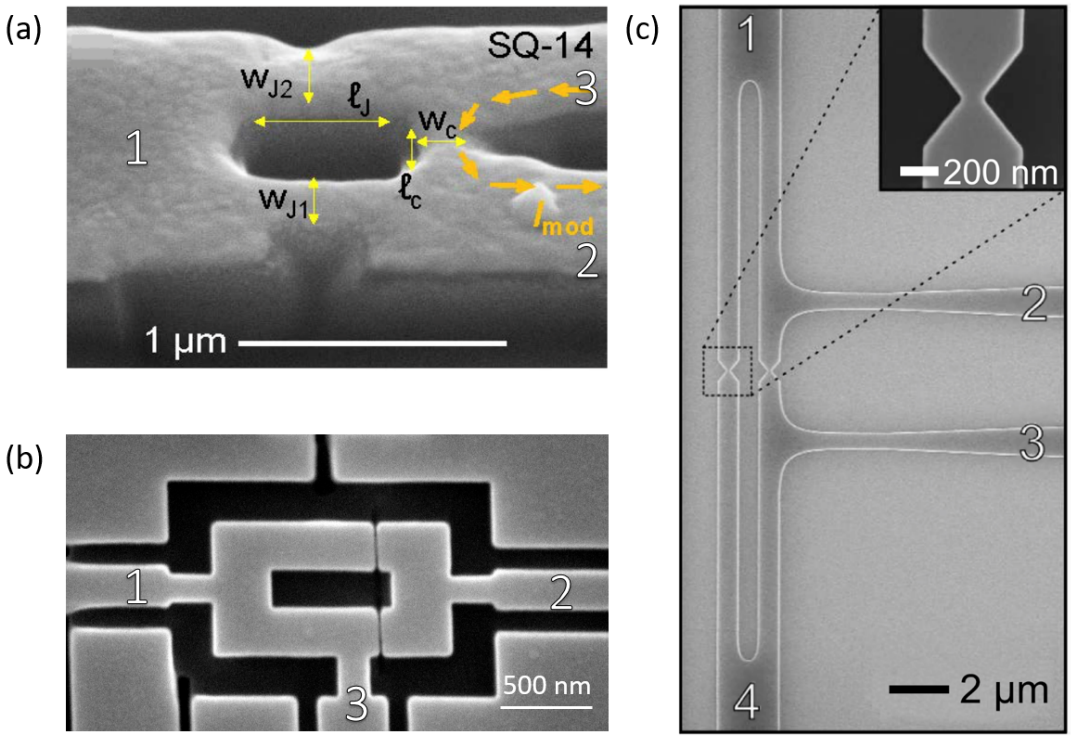

Figure 3.2: The fluxoid state of a SQUID is generally controlled by tuning the applied flux through the SQUID, making use of the SQUID's geometric inductance. However, the fluxoid state can also be altered by running a modulation current to the SQUID, exploiting the SQUID's kinetic inductance. **(a)** This nanoSQUID [24] is biased by running a current between 1 and 2 (or 3). An extra modulation current is applied between points 3 and 2. **(b)** SQUID I is fabricated as part of the two-SQUID device presented in section 5.4. A bias current runs from 1 to 2, and an extra modulation current is applied between 1 and 3. **(c)** A modulation current can also be applied across a junction (Dayem bridge) [23], from 2 to 3. The SQUID is biased by running a current from 1 to 4. When a modulation current is applied between two points, the current does not only take the shortest path. The current is split between both possible paths across the ring according to the relative inductance.

multiple of Φ_0.

Control of the fluxoid state is an integral part of SQUID operation as it allows for optimization of the sensitivity. Usually, the fluxoid state is solely controlled by tuning the applied flux and therefore this process is generally (also in this thesis) referred to as field-biasing. By tuning the applied flux, only the geometric inductance of the SQUID is addressed. However, although less common, the fluxoid state can also be altered by addressing the kinetic inductance of the SQUID. Contrary to L_g, L_k is not coupled to the magnetic field. The kinetic inductance directly relates the current with the phase. For nanostructured devices, the kinetic inductance is at least as large, but often larger than the geometric inductance [23].

To change the fluxoid state using the kinetic inductance, an extra current can be injected along some portion of the ring. This can be either across a junction, Fig. 3.2c, or along a section or the ring's arm, Figs. 3.2a-b. The injected current will induce an

extra circular current proportional to the total inductance. This alters the fluxoid state. This method of fluxoid tuning is useful in multi-SQUID systems as it allows for individual control of the fluxoid states of the SQUIDs. For this reason, this method is applied to the two-SQUID devices that will be presented in section 5.4.

Chapter 4

Indirect Magnetization Measurements

Before we can measure QPFs, we need to verify that we can measure tiny variations in magnetic response. To do so, we measure the critical current of a SQUID with thin Nb film deposited on top as a function of magnetic field and temperature. By comparing the shape of the critical current vs. field curve at different temperatures, we indirectly observe the change in magnetization of this film.

4.1 The Superconducting Transition of a Thin Nb-Film

To test the susceptibility-measuring ability of our SQUIDs, we deposit a thin film of Nb on top of SQUID B using electron-beam lithography (Fig. 4.1). In between the SQUID and Nb film, an insulating layer of SiO_x with a thickness of 80 nm is sputtered. The nanoSQUID itself is also structured out of Nb, having a critical temperature of roughly 7 K (Fig. 4.1b). To measure the Nb film both above and below its superconducting transition, it needs to have a critical temperature below 7 K and above 1.6 K (the lower limit of our cryostat).

In a single run, a Nb film with a thickness of 20 nm was deposited on top of SQUID B and a test substrate. According to [25], in which the same sputtering system as in this research is used, a 20 nm thick film has $T_c \approx 7.8$ K. Measurements on the test film showed a slightly lower critical temperature, $T_c \approx 7.2$ K. Then, this test film was etched until an estimated thickness of 8 nm remained. Measurements on the test substrate showed that the etching process had significantly broadened the superconducting transition: the onset of the transition happened around 4.5 K and despite there being a clear drop in resistance, it did not reach zero within the temperature-operating range of the SQUID. Therefore, it was decided to etch the film on top of SQUID B to a thickness of approximately 9.5 nm. This results in the superconducting transition starting at a higher temperature and the film reaching a lower resistance within the SQUID's range.

To detect the magnetic response of the Nb film going through its superconducting transition, we measure a small section of the SQUID's critical current oscillations as a function of temperature. The exact pattern of the critical current oscillations is always expected to change as a function of temperature, also in the absence of a superconducting film. The critical current of a Josephson junction (and thus of a SQUID) increases with decreasing temperature. However, the location of the critical current minima and maxima

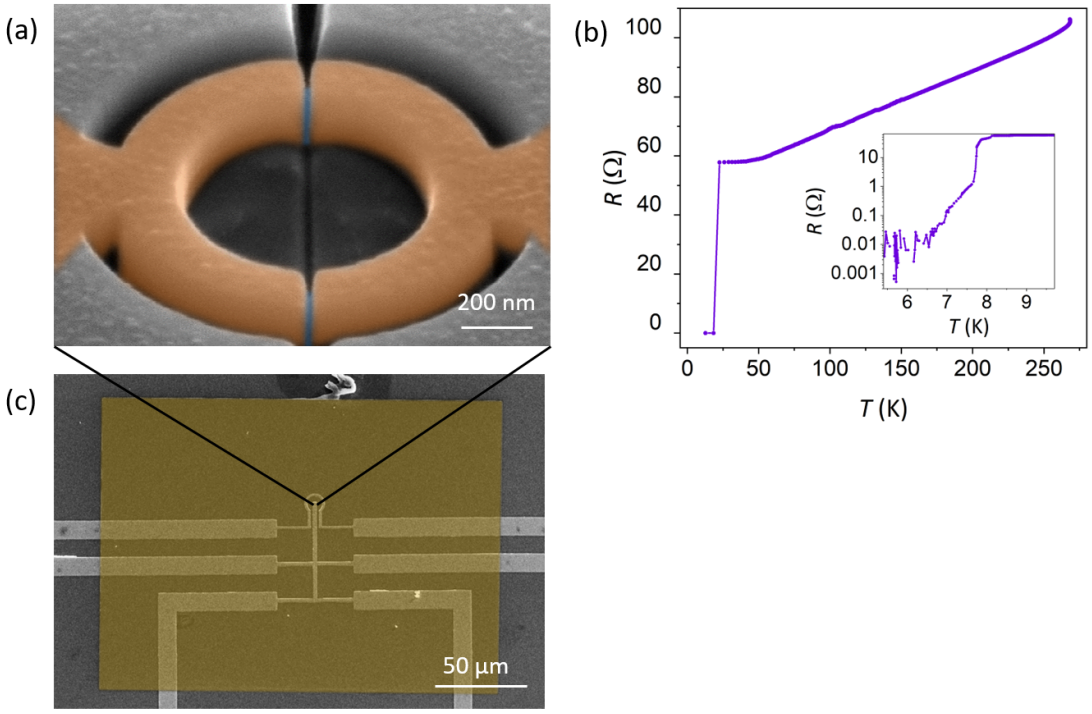

Figure 4.1: **(a)** False-colored SEM image of SQUID B, with the junctions in blue, before the deposition of the SiO_x and Nb layers. **(b)** The temperature vs. resistance curve of SQUID B, after the deposition of the SiO_x and Nb layers. The inset shows that the superconducting transition consists of different steps, corresponding to different parts of the device (contacts, junctions, and arms) becoming superconducting. **(c)** False-colored SEM image of the 9.5 nm Nb film (yellow) on top of SQUID B (and the FC). The SiO_x layer in between the device and Nb film is not visible.

with respect to the magnetic field are temperature-independent, as this solely depends on the SQUID's geometry.

The presence of a superconducting film will have another effect on the critical current oscillations as a function of temperature: the oscillations will be rescaled with respect to the field axis once the film becomes superconducting ($T < T_c$). This can be explained by considering the magnetic susceptibility, which is defined as:

$$\chi = M/H = (B/\mu_0 - H)/H \tag{4.1}$$

H is the externally applied magnetic field, whereas B is the magnetic field sensed by the SQUID. B includes both the applied field and potential magnetic response from a film placed on top of the SQUID*. Above the superconducting transition of the film, the field 'experienced' by the SQUID is equal to the field that is applied: $B/\mu_0 - H = 0$. However, once the film becomes superconducting, it will (partially) screen the applied field and $B/\mu_0 - H < 0$.

This change is visible when comparing the SQUID's critical current oscillations at different temperatures around the film's T_c. As long as $B/\mu_0 - H = 0$, the periodicity of the critical current with respect to the field-axis will remain constant. However, when $B/\mu_0 - H < 0$, the pattern of the critical current oscillations rescales with respect to the applied field-axis. After all, the applied-field axis does no longer represents the fluxoid state of the SQUID. When the pattern is rescaled, the location of the minima and maxima shifts. Such a shift is evidence of the presence of a film that is (partially) screening the applied field.

4.2 Results

To indirectly measure the change in susceptibility of the Nb film, the SQUID + film is cooled in a variable temperature cryostat with three perpendicular magnetic field coils. This system will be referred to as the Vector Magnet (VM). A Keithley current source supplies a bias current of varying magnitude through the SQUID while a Keithley nanovoltmeter records the voltage in a four-point measurement. The external field (perpendicular to the SQUID) in the VM is set to 2.6 mT. This is done using one of the superconducting magnets in this system. The external field value of 2.6 mT yields a maximized AC signal at $T = 2.2$ K. Moreover, the field coil concentric with the SQUID can generate a field varying from approximately -0.2 mT to 0.2 mT by supplying it with a current of ± 600 µA (using a Yokogawa current source).

The field that is generated by the field coil is swept in steps of ± 0.04 mT. At every field value, the bias current through the SQUID is swept and the voltage is recorded. This protocol is repeated at thirteen different temperatures ranging from 1.63 K to 2.33 K. At every temperature, we essentially measure a small section of the SQUID's critical current oscillations, indicated by the yellow rectangle in Fig. 4.2b. This data is shown for four temperatures in Figs. 4.2e-f. For every temperature, an external field vs. critical current curve is extracted, see Fig. 4.2a. The critical current is defined as 9 µV $\leq V \leq$ 11 µV.

*The screening currents induced within the SQUID in response to the externally applied field also contribute to B, but this contribution is generally very small.

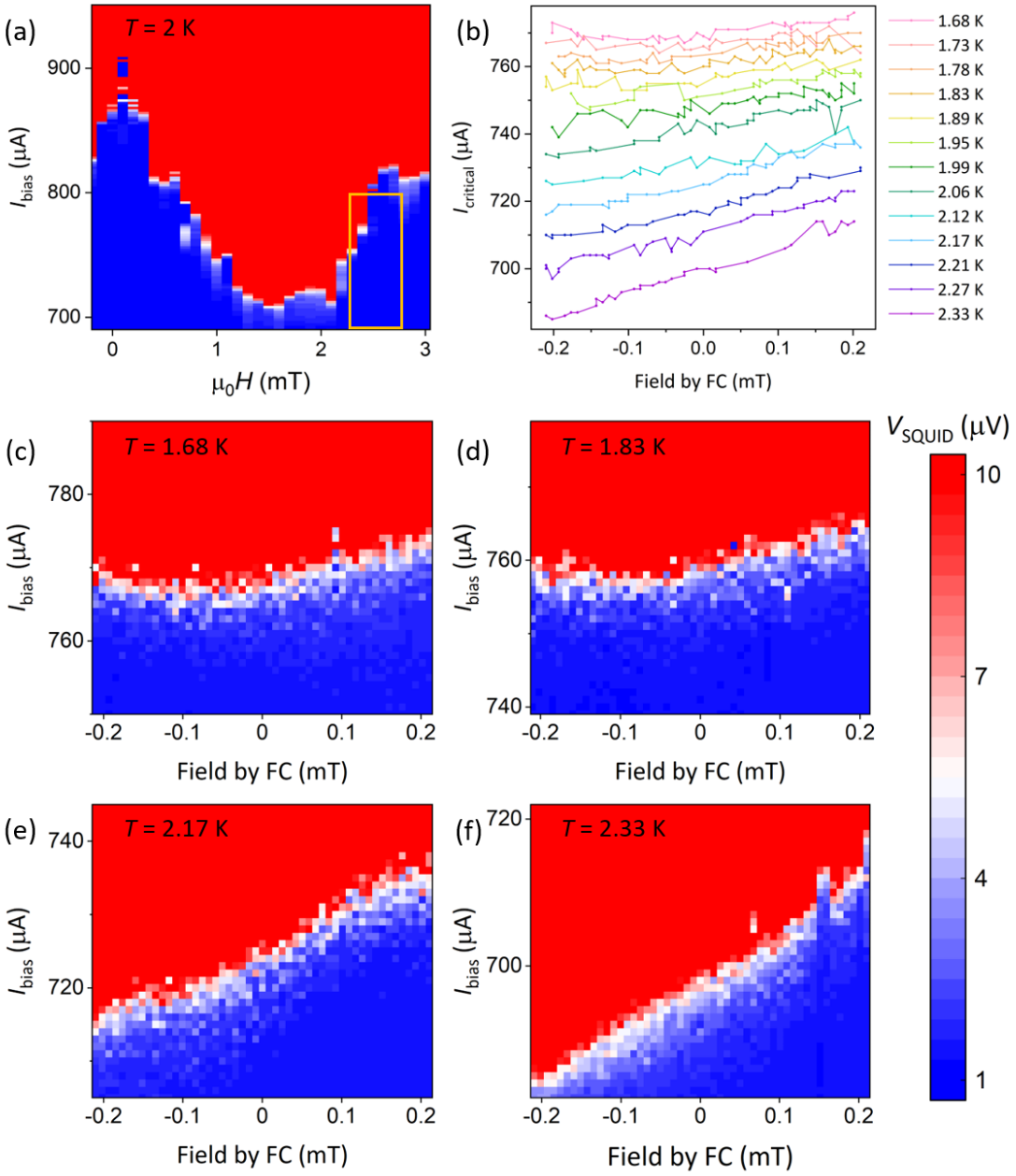

Figure 4.2: **(a)** One period of the critical current oscillations of SQUID B, measured at $T = 2$ K. At the time of measurement, the Nb film was already deposited on top of the device. The yellow rectangle indicates the approximate region that was measured to extract the data that is shown in (b). **(b)** The critical current as a function of the externally applied magnetic field, measured with SQUID B that has a 9.5 nm Nb film on top, at thirteen different temperatures. For the lowest temperatures, the curves show a slight dip. As the temperature is increased, this minimum is no longer visible. This shift in the location of the I_c-minimum with respect to the externally applied magnetic field is a clear indication of the presence of screening currents in the Nb film. **(c)-(f)** show the complete measurements for four temperatures. The white traces indicate the critical current. The external magnetic field was biased at 2.6 mT and the FC was used to sweep around this value. The color bar applies to both (a) and (c)-(f).

For the lowest temperatures, the critical current shows a slight dip in an otherwise relatively flat profile. This corresponds to a minimum in the critical current oscillations. As the temperature is increased, the I_c-profile clearly changes: it becomes progressively more slanted.

Recall that the precise pattern of the critical current oscillations of a SQUID is expected to change as a function of temperature. However, when there is no film with magnetic response deposited on top of the SQUID, the locations of the minima and maxima of the critical current do not change. Only in the presence of a superconducting film that (partially) screens the externally applied field, we expect the locations of the minima and maxima to change as a function of temperature. The data presented in Fig. 4.2 shows a shift in the location of a critical current minimum. Therefore, we can conclude that our SQUID is measuring the change in the film's susceptibility as a function of temperature.

The superconducting transition of this Nb film is expected to be broad because of the etching step. We expect that at all temperatures at which measurements were performed, the film was partially superconducting. But of course, the degree of superconductivity and thus screening capacity increased with decreasing temperature. Seeing as the film is very thin, it would never be able to completely screen the externally applied field. Remarkably, we can detect this very small change in magnetic response with our SQUID. This provides us with confidence that we can also measure QPFs.

Chapter 5

AC Magnetic Susceptibility Measurements

The previous chapter detailed the indirect detection of the change in magnetization of a 9.5 nm Nb film as a function of temperature. For these measurements, the magnetic field was swept over a range much less than the SQUID's period and the magnitude of the critical current was recorded. The results are evidence that our SQUIDs are sensitive to very small changes in magnetic response.

The next step towards our goal to detect QPFs is creating a setup for AC susceptibility measurements of thin films. Chapter 2 explains why a measurement of the differential susceptibility, $\chi = \mathrm{d}M/\mathrm{d}H$, is preferred over a measurement of the regular susceptibility, $\chi = M/H$. This chapter will discuss the AC susceptibility measurement scheme designed for this project and two measurements on thin Nb films.

5.1 Setup

Like the measurements in the previous chapter, the AC susceptibility measurements are performed with a SQUID as a magnetic field sensor, and a FC concentric to the SQUID to locally apply a magnetic field. To operate the SQUID, it is current-biased with a Keithley current source and magnetic field-biased with the cryostat's external field (and FC). A lock-in amplifier is added to the setup. For the experiments in section 5.2 this is an MFLI from Zurich Instruments, and for the experiments in section 5.3 this is a SynkTek MCL1-540.

The output channel of the lock-in amplifier is connected in series with a 1 kΩ resistance and the FC such that an oscillating magnetic field can be generated. Also, a non-zero offset on the output signal creates a time-independent magnetic field that is used to field-bias the SQUID. This field strength can be controlled with a higher resolution compared to the external magnetic fields in the cryostats. The input channel of the lock-in amplifier is connected to the SQUID to measure the in-phase (X) and out-of-phase (Y) components, or equivalently the amplitude (R or ΔV) and phase (ϕ), of the oscillating voltage across the SQUID. This oscillating voltage, of course, results from the oscillating magnetic field and therefore has the same frequency.

At field values of only a few mT, there are only a few vortices in the Nb film. Therefore, we expect little dissipation and the out-of-phase component to be small. However, in all

our AC measurements the out-of-phase component exceeds the in-phase component. The relative magnitude of this component increases with the frequency, which indicates that its non-zero value is caused by cross talk in the electronics.

5.2 AC Response as a Function of Temperature and Bias Current

To test the AC measurement setup, we once again measure films with an expected magnetic response. The first measurement is performed on SQUID B with the 9.5 nm Nb film. This measurement is perfomred in the VM with the setup as described in the previous section.

A SQUID's transfer function, and thus the value of ΔV that we measure, depends on the temperature, external magnetic field strength, and bias current. The magnetic response of the Nb film will be measured as a function of temperature. The values of ΔV at different temperatures will be compared to one another, such that the superconducting transition of the film can be observed. Therefore, we need to ensure that the other two parameters, the bias field and bias current, are optimized such that a maximum response is obtained at every temperature. We assume that the optimal bias field is temperature-independent (an assumption that will be proved wrong near the end of this section). That leads to the following measurement protocol for SQUID B with the 9.5 nm Nb film:

1. At a random temperature in the SQUID's operating range, bias the external magnetic field such that the SQUID operates in the linear regime of the transfer function.

2. At every temperature in the range of interest, sweep the bias current to find the maximum value of ΔV. Record this maximized value and the corresponding bias current.

The protocol is applied to SQUID B with the 9.5 nm Nb film and the results are presented in Fig. 5.1. During this measurement, an oscillating magnetic field with an approximate amplitude of 0.13 mT is applied at a frequency of 12.123 kHz. Initially, the signal strength increases with decreasing temperature. This agrees with the SQUID becoming more sensitive at lower temperatures. Around $T = 2.1$ K, there is a sudden and large drop in ΔV. Possibly, the SQUID's sensitivity decreases below this temperature. However, it is unlikely that the decrease in sensitivity is sufficiently large to account for a drop in signal strength of this magnitude.

Another explanation for the drop in ΔV is an increase in magnetic response (screening) from the Nb film below $T = 2.1$ K. However, it is improbable that this is the only effect at play. First of all, this particular Nb film has a broad superconducting transition that is expected to start at $T = 5$ K and continue below $T = 1.7$ K, where it has small but non-zero resistance. For that reason, it is unlikely that at $T = 2.1$ K the film switches from a little screening ($\Delta V \approx 11$ µV) to screening practically all field strength ($\Delta V \approx 1$ µV). Additionally, it is unlikely that a Nb film with a thickness of 9.5 nm can fully screen the applied field.

Figure 5.1 also shows that the optimized bias current increases as a function of decreasing temperature. This agrees with an increase in critical current as a function of

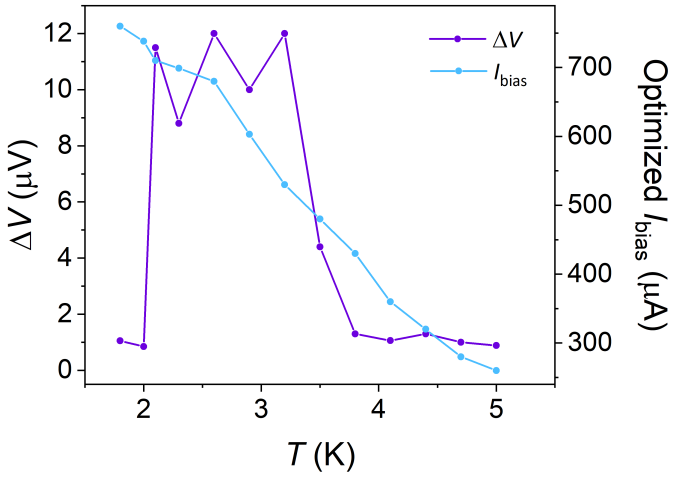

Figure 5.1: The first test of the AC measurement scheme is performed with SQUID B, which has a 9.5 nm Nb film on top. The maximized AC response, ΔV, is plotted as a function of temperature. At every temperature, the response is maximized by tuning the bias current. The optimized bias currents are plotted as well. At first, a decrease in temperature leads to an increase in signal. This is consistent with an increase in the SQUID's sensitivity. Around $T = 2.1$ K, there is a sudden drop in response. It is unlikely that this is solely caused by a sudden and large decrease in the SQUID's sensitivity or screening response of the Nb film.

decreasing temperature.

To further investigate the influence of the SQUID's sensitivity and the screening effects on T vs. ΔV, a reference measurement before film deposition needs to be performed. For SQUID B, this can not be done as the film cannot be removed. Therefore, we make a new SQUID, see Fig. 5.2a. SQUID C is similar to SQUID B, having the same composition and design, only differing in size. SQUID C has a diameter of roughly 700 nm. After measuring the response without film, a Nb film with a thickness of 5 nm is deposited on top of SQUID C, with an insulating layer of SiOx in between, see Fig. 5.2b. According to [25] a Nb with this thickness has a critical temperature of 3 K.

The protocol that is listed above is executed to measure the AC response of the SQUID C as a function of temperature. However, this time the protocol is automated in the cryostat's software. The measurement before film deposition is performed in the VM, whereas the measurement after film deposition is performed in another cryostat, the Teslatron. The Teslatron has one magnetic field coil that is parallel to the SQUID's ring. During these measurements, an oscillating field with an amplitude of approximately 0.13 mT was applied at a frequency of 12.123 kHz. The results are presented in Figs. 5.2c-d.

Fig. 5.2b shows that before film deposition, there is a peak in the response around $T = 2.6$ K. This might seem to suggest that the SQUID is most sensitive at this temperature. If this curve truly represents the sensitivity of SQUID C as a function of temperature, we expect that after film deposition, the curve would follow the same shape until the film becomes superconducting, $T_c \approx 3$ K. Below this temperature, we expect the signal to be lower compared to the signal before film deposition. The exact shape of the curve below T_c would depend on the degree of screening that can be achieved by the film. The difference in ΔV at each temperature between the measurement before and after the film deposition would be indicative of the degree of screening, and thus the susceptibility.

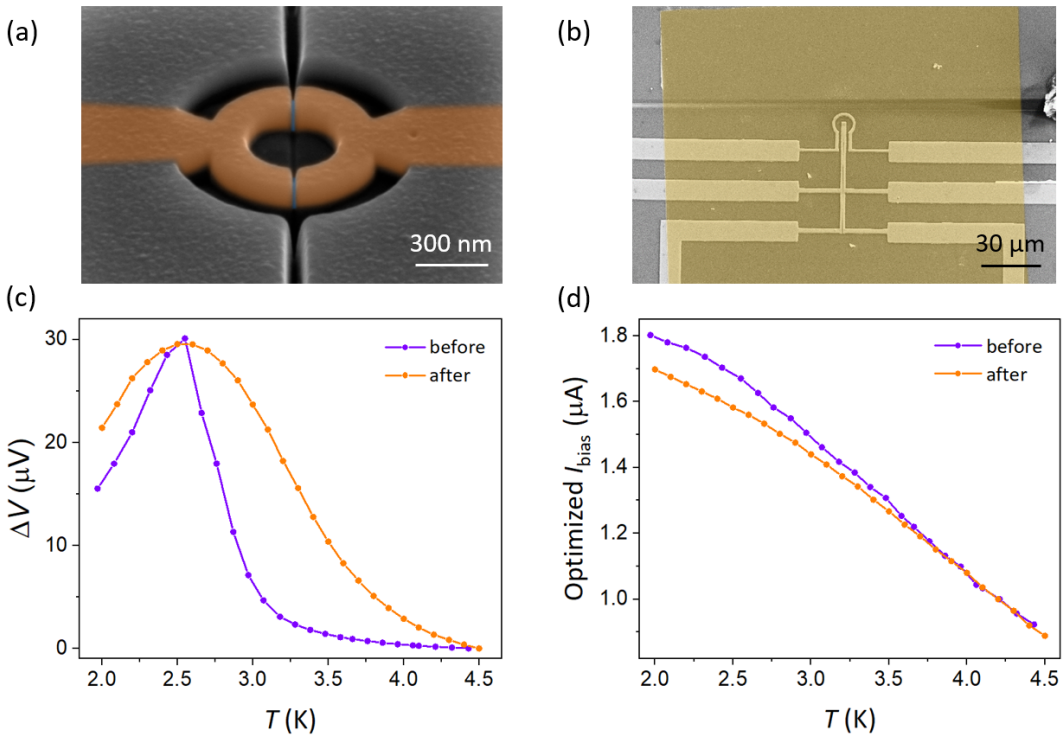

Figure 5.2: **(a)** False-colored SEM image of SQUID C, with the junctions in blue, before the deposition of the SiO_x and Nb layers. **(b)** False-colored SEM image of the 5 nm Nb film (yellow) on top of SQUID C (and the FC). The SiO_x layer in between the device and Nb film is not visible. **(c)** The maximized response, ΔV, of SQUID C as a function of temperature, both before (purple) and after (orange) the deposition of the 5 nm Nb film. The response is maximized at every temperature by tuning the bias current. The optimized bias currents are plotted in **(d)**. The AC response does not follow expectations: the response after film deposition is higher than the response before film deposition at almost all temperatures. This can be explained by the fact that the SQUID's IV characteristics change during film deposition. The peak in response around $T = 2.6$ K can be explained by the fact that both before and after film deposition, the external field strength was optimized while the system was at approximately $T = 2.5$ K.

However, as the results indicate, there is no such relation between the before and after curves.

We notice that after film deposition, a peak in the response occurs at approximately the same temperature as before film deposition. This might be interpreted as evidence for a maximum in the transfer function of SQUID C at this temperature. However, we argue that there is a better explanation for this observation.

Recall that the current measurement protocol is based on the assumption that the magnetic field strength that yields maximum response is temperature-independent. Therefore, the magnetic field was optimized only at a single temperature. This assumption is wrong; the linear region of the transfer function is not necessarily located at the same magnetic field strength for different temperatures. This conclusion is reinforced by the fact that for both measurements (before and after film deposition) the external field was optimized when the system was $T \approx 2.5$ K.

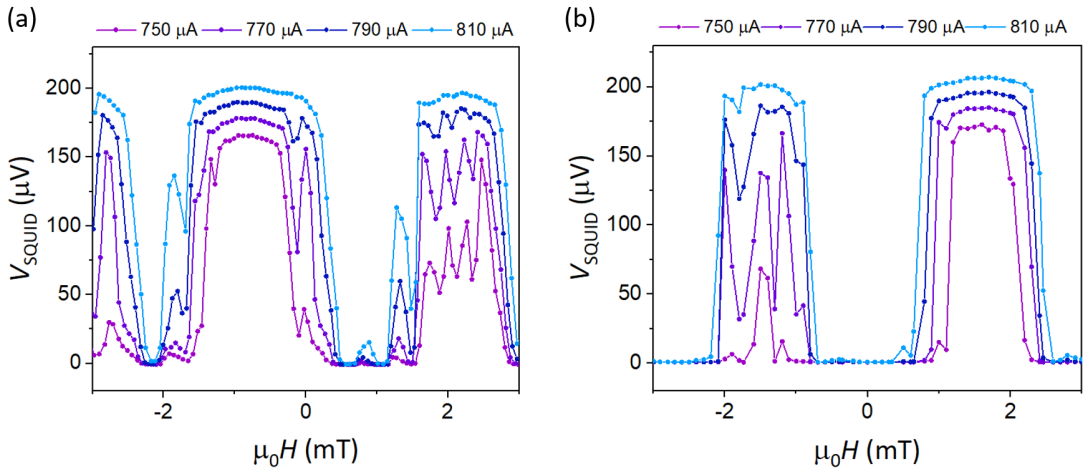

Figure 5.3: Transfer functions of SQUID B for four different bias currents at $T = 2$ K before the deposition of the Nb film (but after the deposition of the SiO_x layer) **(a)**, and after the deposition of the Nb film **(b)**. The measurements presented in **(a)** were performed in the PPMS, whereas the measurements presented in **(b)** were performed in the VM. It is unknown whether the field orientation in these two systems is identical, or rotated 180 degrees. Even when a possible mirroring of one of the field axes is taken into account, it is evident that the film deposition has changed the IV characteristics of the SQUID.

Also, Fig. 5.2c shows that the response after film deposition exceeds the response before film deposition at almost all temperatures. This contradicts our expectation that the signal after film deposition is either equal to (above T_c of the film) or lower than (below T_c of the film) the signal before film deposition. An explanation of this observation can be a change in IV characteristics of the SQUID after film deposition. This also clarifies why the optimized bias current as a function of temperature is not identical before and after film deposition, see Fig. 5.2d.

After we performed these AC measurements on SQUID C, we realized that our SQUIDs are likely changing during the film deposition process. This led to a reexamination of data of both SQUID B and SQUID C. Fig. 5.3 shows a selection of transfer functions of SQUID B before and after film deposition.

The measurements in Figs. 5.3 were performed in different cryostats. The measurements before film deposition were performed in the PPMS. Contrary to the magnetic field coils of the VM and Teslatron, the coil in this cryostat cannot operate in a persistent mode, which adds to the uncertainty in the magnetic field strength. It is unknown whether the magnetic field orientation of these systems is identical, or rotated 180 degrees. Therefore, it might be that for one of the measurements, the field axis needs to be mirrored in $\mu_0 H = 0$ mT.

Fig. 5.3 clearly illustrates that the transfer functions of SQUID B have changed after film deposition, also when a possible mirroring of and shift in one of the field axes is taken into account. Although not shown, this is also true for other temperatures and bias currents. Also, the transfer functions of SQUID C change after film deposition.

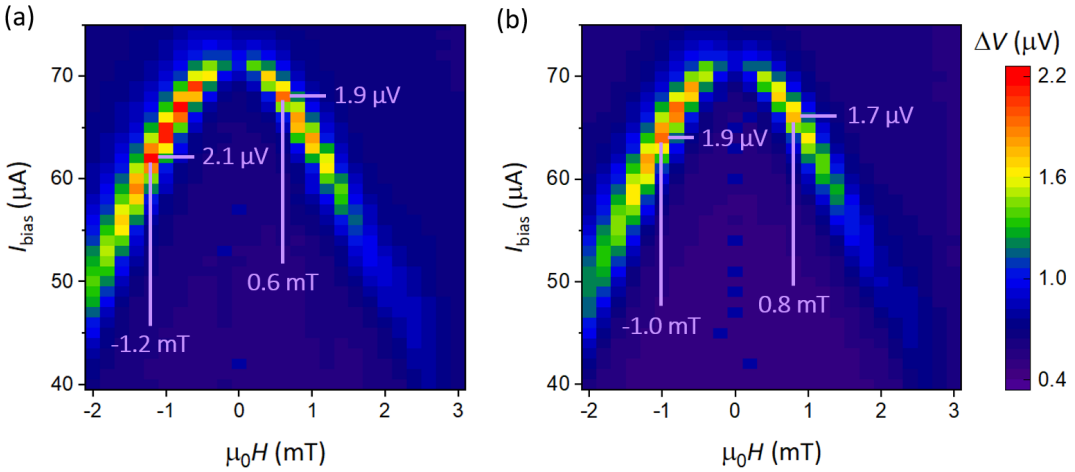

Figure 5.4: A region of SQUID II's parameter space is swept twice at $T = 1.7$ K. The AC response, ΔV, is recorded as a function of the external magnetic field and bias current. The first sweep, **(a)**, shows two maxima at -1.2 mT and 0.6 mT. The results from the second sweep, **(b)**, show a shift of 0.2 mT of these maxima. This falls within the uncertainty range of the cryostat's magnet. The difference in AC response magnitude among the two measurements can be explained by under-sampling.

A possible explanation for the changing IV-characteristics is oxygen migration between the SQUID (Nb) and insulating layer (SiO_x). The film of interest is placed on top of the SQUID by electron-beam lithography and sputtering. Both processes heat the SQUID and possibly cause the migration of oxygen to and from the SQUID. This changes the superconductor and thus the SQUID. A solution would be to cap the SQUID with a thin layer of an unreactive metal such as platinum. Such a capping layer would inhibit oxygen migration, making the SQUID a more stable sensor. No SQUIDs with capping layers like this have been fabricated for this thesis.

5.3 AC Response as a Function of Bias Current and Magnetic Field

One of the conclusions from the AC measurements presented in the previous section is that magnetic field biasing is temperature-dependent. This enlarges the parameter space that must be searched to find the maximized response.

To verify that this parameter space has reproducible maxima, we fabricate a new device, SQUID II, and perform sweeps of identical regions of the parameter space, see Fig. 5.4. This SQUID is part of a two-SQUID device that will be further elaborated on in the next section. These automated AC measurements are performed in the Teslatron with a magnetic field amplitude of 0.5 mT and at a frequency of 27 Hz.

The sweeps of the parameter space show an almost identical pattern. There is a shift of 0.2 mT between the two sweeps. This shift corresponds to the resolution of the magnetic field that is swept using the external magnet in the cryostat. This limited resolution and the fact that there might be a remnant current in the superconducting magnet of the cryostat explain the presence of this shift.

The maxima in amplitude (ΔV) are not only shifted but also slightly differ in magnitude among the two sweeps. This can be explained by the fact that the amplitude is the average of a number of statistically independent samples of the SQUID's response, as recorded by the lock-in amplifier. For the data in Fig. 5.4 the number of samples was $N = 20$. By increasing N, it is expected that the response among different measurements shows smaller deviations.

5.4 Two-SQUID Measurement Protocol

The measurements with SQUIDs B and C have taught us how to properly bias SQUIDs and perform AC susceptibility measurements. The next step toward multi-SQUID correlation measurements, is designing a protocol for AC susceptibility measurements as a function of time with two SQUIDs. Figure 5.5 shows the device that was fabricated for this purpose. It consists of a FC with a radius of 30 µm and two rectangular, or 'letterbox-type', SQUIDs. Apart from the modulation line, SQUID I and II are identical in design. Therefore, the magnetic field strength that maximizes the response of SQUID II is close to the field strength that maximizes the response of SQUID I. The expected difference in field strength can be compensated for with the help of the modulation line on SQUID I (section 3.3).

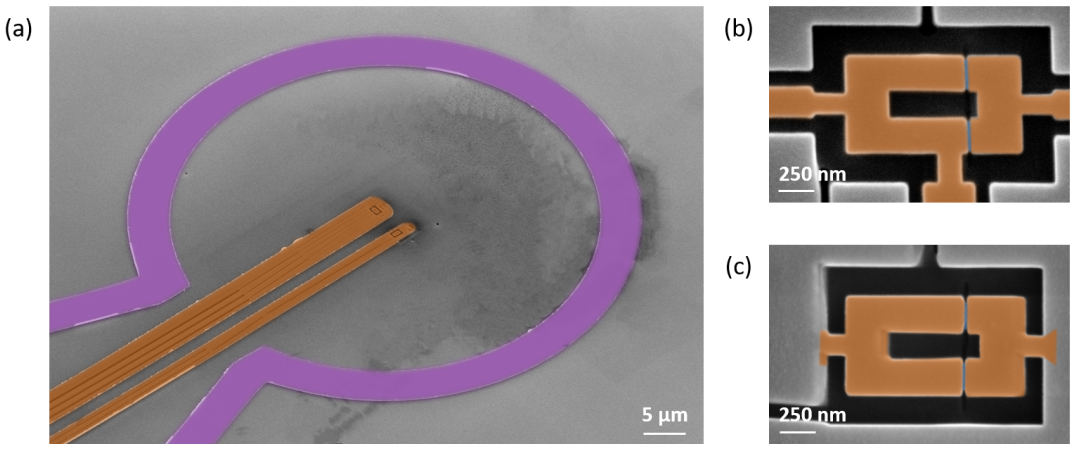

Figure 5.5: False colored SEM images of the two-SQUID device. **(a)** The FC (purple) has a diameter of 60 µm. SQUID I is located on the tip of the left 'finger' (orange) and SQUID II is located on the tip of the 'right' finger (orange). SQUID I **(b)** has an extra contact compared to SQUID II **(c)** such that a modulation current can be run through it. The junctions are depicted in blue.

To simultaneously measure the AC magnetic response of two SQUIDs as a function of time, we propose the following setup. To operate this two-SQUID device, multiple lock-in amplifier channels are required. The SynkTek seems a suitable option. The output signal of the first module will be connected in series with a resistance to the FC, such that an oscillating field can be generated. Two inputs of the same module will be connected across the two SQUIDs to record their oscillating voltages (ΔV) and phases (ϕ). To bias the SQUIDs and operate the modulation line on SQUID I, either current sources like the Keithley or Yokogawa, or the output channels of the other SynkTek modules can be used.

To detect the magnetic response of a Nb film going through its superconducting transition (sections 4.2 and 5.2), we performed measurements at a range of temperatures. On the other hand, to detect QPFs, we can measure at a single temperature. The following measurement protocol will be executed after deposition of the film of interest (a disordered superconductor):

1. Perform a parameter space sweep (ΔV as function of I_{bias} and H) for SQUID II, as was done in section 5.3.
2. Based on the parameter space sweep, field- and current-bias SQUID II at the values that yield the maximum AC response.
3. Sweep I_{bias} through SQUID II and record the response, ΔV, while H remains at the value that optimizes the response of SQUID II.
4. Current-bias SQUID I with the value that maximizes its response.
5. While current-biasing SQUID I, sweep the modulation current, I_{mod} and record the response.
6. Apply the modulation current magnitude that maximizes SQUID I's response. Now, both SQUIDs are properly biased.
7. Measure the response of both SQUIDs as a function of time, ensuring that the number of samples per measurement, N, is sufficiently high.

No two-SQUID measurements were performed with this device. However, with this protocol in place, the next step is to deposit a MoGe film on top of this device and measure response as a function of time.

Chapter 6

Conclusion & Outlook

This thesis was aimed at developing a measurement scheme that could help answer a fundamental open question about QPTs: what are the characteristic length and time scales that govern the QPFs around these transitions? A type of QPT can be found in disordered superconductors: the SIT. The QPFs of a SIT can be detected by locally probing the phase coherence of the Cooper pairs that exist on either side of the transition.

To locally probe phase coherence, we fabricated nanoSQUIDs with concentric FCs onto which disordered superconductors can be directly deposited. The combination of a nanoSQUID and a FC allows for the local measurement of AC magnetic susceptibility, which is a measure of the phase coherence. The final goal is the production of multi-SQUID devices that can measure AC susceptibility at multiple locations on a film, separated by different distances. By examining the correlations between the values measured by the different SQUIDs at each moment in time, we can infer information about the characteristic length and time scales of the QPFs.

The first step towards these multi-SQUID devices was made by fabricating single-SQUID devices. With the first SQUID, the magnetic response of a 9.5 nm Nb film going through a relatively broad superconducting transition was indirectly detected. These measurement results seem to verify that our SQUIDs are remarkably sensitive to tiny changes in the magnetic response of a film that is deposited directly on top. This provides us with confidence that we can measure the small signal of QPFs.

The next step was the development of a single-SQUID AC susceptibility measurement scheme. The first tests of this scheme were performed on the SQUID with the 9.5 nm Nb film. The AC response as a function of temperature showed a large and sudden drop that could not be explained by the broad superconducting transition of this Nb film. A new SQUID was fabricated and its AC response as a function of temperature was measured before and after the deposition of a 5 nm Nb film with a steep superconducting transition. From the results, it was concluded that during the AC susceptibility measurements on both the 9.5 nm and 5 nm Nb film, the SQUIDs were not properly field-biased. Therefore, the values measured at different temperatures could not be compared to one another. Apparently, the magnetic field strength that optimizes a SQUID's response is temperature-dependent.

Moreover, by comparing measurements from before and after film deposition, it was

concluded that film deposition changes the IV characteristics of our SQUIDs. Therefore, calibration measurements from before film deposition are unusable. The SQUIDs are expected to change because of oxygen migration between the SQUID (Nb) and insulating layer (SiO_x) that occurs when the device is heated during film deposition.

Another SQUID, without a film deposited on top, was used to map the parameter space of the SQUID. From these results, it could be concluded that the AC SQUID response as a function of external magnetic field and bias current is stable in time. This means that our process of SQUID biasing is reproducible.

Finally, a two-SQUID device was fabricated. One of the SQUIDs of this device has a modulation line, such that both SQUIDs can be properly biased. A measurement setup and protocol to measure AC susceptibility with these two SQUIDs simultaneously was outlined. No two-SQUIDs measurements were performed.

The next step would be to verify the two-SQUID measurement protocol by measuring a film with a known magnetic response, like Nb. Afterwards, a disordered superconductor like MoGe could be measured with this device and protocol, hopefully detecting QPFs. Of course, to obtain valuable information about the spatial and temporal nature of QPFs, the setup must be expanded to measure with three or more SQUIDs.

Bibliography

[1] Lee, H.-L., Carini, J. P., Baxter, D. V., Henderson, W. & Grüner, G. Quantum-Critical Conductivity Scaling for a Metal-Insulator Transition. *Science* **287** (2000).

[2] Kumar, P., Nosov, P. A. & Raghu, S. Interaction effects on quantum Hall transitions: Dynamical scaling laws and superuniversality. *Phys. Rev. Res.* **4** (2022).

[3] Coldea, R., Tennant, D. A., Wheeler, E. M., Wawrzynska, E., Prabhakaran, D., Telling, M., Habicht, K., Smeibidl, P. & Kiefer, K. Quantum Criticality in an Ising Chain: Experimental Evidence for Emergent E 8 Symmetry. *Science* **327** (2010).

[4] Rüegg, C., Normand, B., Matsumoto, M., Furrer, A., McMorrow, D. F., Krämer, K. W., Güdel, H. U., Gvasaliya, S. N., Mutka, H. & Boehm, M. Quantum Magnets under Pressure: Controlling Elementary Excitations in $TlCuCl_3$. *Phys. Rev. Lett.* **100** (2008).

[5] Hebard, A. F. & Paalanen, M. A. Magnetic-field-tuned superconductor-insulator transition in two-dimensional films. *Phys. Rev. Lett.* **65** (1990).

[6] Wang, T., Pan, Z., Ohtsuki, T., Gruzberg, I. A. & Shindou, R. Multicriticality of two-dimensional class-D disordered topological superconductors. *Phys. Rev. B* **104** (2021).

[7] Kremen, H. K. Y. L. L. T. I. B. N. T. A. F., A. & Kalisky, B. Imaging Quantum Fluctuations near Criticality. *Nature Physics* **14** (2018).

[8] Fisher, M. P. A. Quantum phase transitions in disordered two-dimensional superconductors. *Phys. Rev. Lett.* **65** (1990).

[9] Yazdani, A. & Kapitulnik, A. Superconducting-Insulating Transition in Two-Dimensional a-MoGe Thin Films. *Phys. Rev. Lett.* **74** (1995).

[10] Sachdev, S. & Keimer, B. Quantum criticality. *Physics Today* **64** (2011).

[11] Ghosal, A., Randeria, M. & Trivedi, N. Role of Spatial Amplitude Fluctuations in Highly Disordered s-Wave Superconductors. *Phys. Rev. Lett.* **81** (1998).

[12] Dubi, Y., Meir, Y. & Avishai, Y. Nature of the superconductor-insulator transition in disordered superconductors. *Nature* **449** (2007).

[13] Stewart, M. D., Yin, A., Xu, J. M. & Valles, J. M. Superconducting Pair Correlations in an Amorphous Insulating Nanohoneycomb Film. *Science* **318** (2007).

[14] Nguyen, H. Q., Hollen, S. M., Stewart, M. D., Shainline, J., Yin, A., Xu, J. M. & Valles, J. M. Observation of Giant Positive Magnetoresistance in a Cooper Pair Insulator. *Phys. Rev. Lett.* **103** (2009).

[15] Dutta, S., Jesudasan, J. & Raychaudhuri, P. Magnetic field induced transition from a vortex liquid to Bose metal in ultrathin-MoGe thin film. *Physical Review B* **105** (2022).

[16] Bishop-Van Horn, L., Mueller, E. & Moler, K. A. Vortex dynamics induced by scanning SQUID susceptometry. *Physical Review B* **107** (2023).

[17] Božović, I., He, X., Wu, J. & Bollinger. Dependence of the critical temperature in overdoped copper oxides on superfluid density. *Nature* **536** (2016).

[18] Persky, E., Sochnikov, I. & Kalisky, B. Studying Quantum Materials with Scanning SQUID Microscopy. *Annual Review of Condensed Matter Physics* **13** (2022).

[19] Vasyukov, A. Y. E. L. e. a., D. A scanning superconducting quantum interference device with single electron spin sensitivity. *Nature Nanotech* **8** (2013).

[20] Rog, M. *SQUID-on-tip Magnetic Microscopy using Tunneling-Based Height Control.* Msc thesis, Leiden University (2022).

[21] José Martínez-Pérez, M. & Koelle, D. NanoSQUIDs: Basics & recent advances. *Physical Sciences Reviews* **2** (2017).

[22] Braginski, A. & Clarke, J. *The SQUID Handbook Vol. I Fundamentals and Technology of SQUIDs and SQUID Systems* (WILEY-VCH, 2004).

[23] McCaughan, A., Zhao, Q. & Berggren, K. NanoSQUID operation using kinetic rather than magnetic induction. *Scientific Reports* **6** (2016).

[24] Lin, J., Linek, J., Kleiner, R. & Koelle, D. NanoSQUIDs from YBa2Cu3O7/SrTiO3 superlattices with bicrystal grain boundary Josephson junctions. *Nanoscale* **12** (2020).

[25] Cirillo, C., Rusanov, A., Bell, C. & Aarts, J. Depairing current behavior in superconducting Nb/$Pd_{81}Ni_{19}$ bilayers. *Phys. Rev. B* **75** (2007).